

1 **Revision 2**

2 **Vaterite – interpretation in terms of OD theory and its next of kin**

3 **EMIL MAKOVICKY**

4 Institute of Geoscience and Natural Resource Management, University of Copenhagen,
5 Østervoldgade 10, 1350 Copenhagen, Denmark

6 E-mail: emilm@ign.ku.dk

7 **ABSTRACT**

8 The polytypic structures of vaterite, CaCO_3 , described in recent literature, have been reinterpreted
9 in terms of the OD (order-disorder theory) which allows us to explain and systematize all the
10 observed and predicted polytypes of the mineral in a unified fashion. In terms of this theory, the
11 structure consists of OD layers which comprise a layer of calcium coordination polyhedra and the
12 attached halves of the standing CO_3 groups. The two-sided layer group of symmetry of the OD
13 layer is $c2/m$ whereas the interlayer symmetry operations are three two-fold rotation axes at 120° to
14 one another, as well as a mirror plane in the common layer boundaries and partial c glide planes
15 perpendicular to the boundary. Depending on the orientation of the active two-fold rotation axis
16 with respect to the above-defined layer mesh, performed independently in each stacking step,
17 maximally ordered simple stacking sequences $P6_122$, $P6_522$, $C2/c$, $C2/c2/m2_1/m$ and a more
18 complicated sequence $P3_12$ or $P3_22$, as well as a number of complicated or disordered sequences is
19 obtained (before eventual relaxation to a subgroup of a particular space group). A perfect copy of
20 the vaterite OD layer occurs in the structures of the bastnäsité - synchysite polysomatic series of
21 fluorocarbonates. In these structures, the *REE* layers, configurationally analogous to the Ca-based
22 OD layer, have layer symmetry $p32$ and their stacking does not lead to polytypism and OD
23 phenomena; these are generated on the Ca-based OD layers.

24 **Keywords:** vaterite, calcium carbonate, polytypes, OD theory

25 **INTRODUCTION**

26 The highly disordered crystal structure of the third polymorph of CaCO_3 , *vaterite*, has
27 been object of several interpretations, in widely different space groups [e.g., Meyer
28 (1969), the substructure by Kamhi (1963), Medeiros et al. (2007) and Le Bail et al.
29 (2011)]; the bulk of recent information was summarized by Demichelis et al. (2012,
30 2013). These authors and Mugnaioli et al. (2012) investigated vaterite respectively by
31 *ab initio* calculations and by automated electron diffraction experiments, proposing
32 again different crystal structures. Another group which published the results of *ab*
33 *initio* calculations is Wang and Becker (2009), with a structure proposal closest to
34 that of Demichelis et al. and a good summary of previous investigations.

35 All three groups of authors, however, describe the same type of calcium layers and
36 the same type of the loosely configured interspersed CO₃ layers in their proposed
37 structures. Only one type of each layer is present if we disregard small distortions in
38 individual structures, produced by structure relaxation in a particular space group.
39 Mugnaioli et al. (2012) undertook a ‘normal-course’ crystal structure determination
40 whereas Wang and Becker (2009) and Demichelis et al. (2012, 2013) do not report a
41 potential source of their configurations, concentrating in detail on the structure
42 descriptions by means of layer shifts and changing orientation. These, in principle
43 identical, and very plausible results, and the hitherto generally unacknowledged
44 presence of such layers in the fluorocarbonates of the batnäsite-synchisite
45 polysomatic series are the rationale behind this contribution.

46 Perusal of these results led the present author to the application of the OD (order-
47 disorder) theory initiated by Dornberger (1956,1966) and further advanced by, e.g.,
48 Āurovič (1997) and Merlino (1997). A short review of fundamental notions of the
49 OD theory is given in the appendix; we shall not repeat them here, and it is
50 recommended to start reading the appendix before the paper itself. The crystal
51 structure of vaterite lends itself both to one-layer and two-layer OD description. The
52 3D results of the description in terms of one OD layer type are easier to comprehend
53 and it is the approach adopted here.

54 **THE OD LAYERS AND THEIR STACKING SEQUENCES**

55 The crystal structure of vaterite consists of alternating layers of Ca
56 polyhedra (CN = 6 – 8) and ‘standing’ CO₃ groups, the latter with one edge of every
57 coordination triangle parallel to the layer stacking direction (Fig. 1). Calcium cations
58 form a fairly regular hexagonal net, and on both sides of it every second triangle of
59 the Ca net is accompanied by a CO₃ group. In their own ‘carbonate’ layer, these
60 groups are disposed along three sides of a hexagonal prism with a height equal to the
61 O – O edge of the CO₃ triangle and with alternating sides of the prism unoccupied,
62 with overall point group symmetry $\bar{6}$ (Fig. 2). The hexagons form an openwork layer
63 by sharing their sides but six of them always surround and enclose a smaller ditrigon,
64 which has three CO₃ triangles pointing toward its center, and three alternate triangles
65 pointing outward, positioned in its vertices (Fig. 2). The cation sheet alone
66 approximates closely the two-sided $p6/mmm$ layer group of symmetry; the CO₃ layer
67 alone approximates symmetry $p-62m$ (with 2₁ axes and g planes situated between,
68 and parallel to, the twofold rotation axes of the two-sided layer group of symmetry).

69 The periodicities of the idealized carbonate layer, and of the carbonate – Ca pair of
70 layers, form a supercell of the idealized periodicity of the Ca net itself; the former are
71 related to the latter by the matrix

$$\begin{pmatrix} 1 & -1 \\ 2 & 1 \end{pmatrix}$$

74 and the orientation of the respective mesh differs by 30° . This is the two-dimensional
75 cell used in the subsequent text.

76 The *OD layer* will be modeled as the central plane of Ca ions, with the ‘inner’ halves
77 of the standing CO_3 groups on both sides added (Fig. 3). The ‘outer’ or peripheral
78 halves of CO_3 belong to the adjacent OD layers; the C atoms, and the oxygen atoms
79 at the same height levels, are shared by two adjacent OD layers, i.e., they represent a
80 layer boundary. The CO_3 configurations across the Ca plane are not mirror-related;
81 they are related by ‘horizontal’ two-fold axes in the Ca plane, and preserve one of the
82 vertical mirror planes of the Ca plane, which becomes common to all three just
83 mentioned subunits of the OD layer (i.e., to the Ca net and two halves of adjacent
84 carbonate layers) (Fig. 3). The resulting layer symmetry group of the OD layer is
85 $c2/m$; the centration results from application of a rectangular cell to a hexagonal motif
86 of the Ca layer. If we select m as (10.0) of the hexagonal net of the carbonate – Ca
87 pair, defined in the previous paragraph, then the a parameter of the *centred*
88 rectangular OD layer cell will be the next longer Ca-Ca distance (a_2 of the carbonate
89 hexagonal motif), and the b parameter will ideally be equal to $2a \cos 30^\circ$, i.e., the
90 vector $2\mathbf{a}_1 + \mathbf{a}_2$ of the 2D hexagonal cell. Layer group symmetry $2/m$ of λ (i.e.,
91 intralayer; see the appendix) operations is significantly reduced in comparison to the
92 symmetries of the three individual parts which together constitute the OD layer.

93 The interlayer *sigma* operations, which transform the n th OD layer into $(n+1)$ st OD
94 layer, are determined by the configurations of the CO_3 layer straddling the boundary
95 of two OD layers. In the ideal model, without relaxation pertinent to a particular
96 polytype, its vertical mirror planes are (10.0), (01.0) and (1-1.0) of the carbonate net,
97 and two-fold axes are in the direction of its crystallographic a_1 , a_2 and a_3 axes (Fig.
98 4). These axes are polar, the $+a_i$ and the $-a_i$ direction is always different. The $p-6 2 m$
99 symmetry includes three-fold axes, and a ‘horizontal’ reflection plane. In terms of the
100 layer-reversing *rho* operations, it is the actions of the latter reflection plane, and of
101 the twofold axes, which propagate the n th layer into the $(n+1)$ st layer.

102 With respect to the *lambda* mirror plane in the OD layer (symmetry $2/m$), there are
103 two possible orientations of the *sigma* two-fold axes (and associated vertical mirror
104 planes) situated in the layer boundary. When the two-fold axis follows one of the
105 diagonals of the centered cell of the OD layer, which in the above defined orientation
106 of the OD layer, $m \parallel (10.0)$, can be a hexagonal a_1 or a_3 axis, a combination of the 2-
107 fold rotation with the internal symmetry of the OD layer results in the $(n+1)$ st layer
108 being rotated by 60° against the n th one (Fig. 4). An additional, *tau-sigma* operation
109 results from these operations; it is a partial glide plane c_2 (*this symbol indicates a full*
110 *translation period from a layer to a layer as a translation component*) which is
111 perpendicular to the two-fold axis performing the transformation.

112 Application of the same orientation of the acting (*sigma*) two-fold rotation axis to
113 each consecutive OD layer results in the generalization of the partial 6_1 or 6_5
114 operation (one 60° turn) into a general one, producing a six-layer polytype $P6_1$ (or 5) 22 ,
115 one of the vaterite polytypes with a maximum degree of order (MDO polytype). The
116 MDO polytype is defined as a polytype in which the same *sigma* operation is applied
117 at each derivation step. The $P6_522$ structure is the polytype derived by Wang and
118 Becker (2009) and Demichaelis et al. (2012, 2013).

119 Application of the two-fold axis which has the a_1 orientation on the n th level,
120 followed by the axis in the a_3 orientation in the $(n+1)$ st level, then a_1 again, etc.,
121 always defined for the new orientation of the layer mesh, results in a two-layer $C2/c$
122 structure, this being another MDO polytype. Mugnaioli et al. (2012) determined the
123 $C2/c$ structure from electron diffraction data. They chose a monoclinic two-layer unit
124 cell in which each OD layer has the m direction as a cell diagonal, with the resulting
125 cell dimensions equal to a 12.17 Å, b 7.12 Å, c 9.47 Å, β 118.94°, d_{001} 8.29 Å.
126 Because of the pseudo-hexagonality of the individual components of the OD layer, the
127 dimensions of their centered $a \times b$ cell are actually equal to those of the here
128 described OD layer cell. Thus far, it is the only successful structure determination on
129 vaterite, even if the R_1 factor for the electron diffraction data was as high as 37.6 %.
130 This $C2/c$ sequence can be complicated by stacking errors when, in some instances, a
131 'wrong' orientation of the two-fold axis (twice the a_i orientation with the same i) is
132 active on a certain level, turning a consecutive part of the layer stack by 60° off the
133 periodic sequence and eventually resulting in a quasi-random sequence of small $C2/c$
134 blocks.

135 For the OD layer with the $c2/m$ layer mesh oriented with the short $a_{OD\ layer}$ parameter
136 parallel to the a_2 axis of the hexagonal mesh of the carbonate interlayer (Fig.4), and
137 the interlayer two-fold rotation axis also parallel to a_2 , the action of the latter axis,
138 combined with the symmetry of the OD layer, results in the same effect as the action
139 of the ‘horizontal’ reflection plane. With the same naming of axes, a *two-layer*
140 orthorhombic structure results, $C2/c2/m2_1/m$ for an unrelaxed MDO structure. It
141 should be noted that in this case, relation between two adjacent ‘OD layers’ differs
142 from the previous case.

143 A one-layer polytype with a simple translational stacking of OD layers does not exist
144 because the ditrigonal configurations of the carbonate half-layer on the bottom face
145 of the OD layer are inverted against those on the top face by the action of the $2/m$
146 symmetry of the OD layer. A threefold twinning *inside an individual OD sheet* is
147 hindered by steric problems. When, in a given orientation, a set of triangular CO_3
148 groups is aligned coincident with the mirror plane of the $c2/m$ group, the
149 corresponding sets at $\pm 120^\circ$ to the former one decompose into two parallel, fairly
150 distant subsets, those from the top and from the bottom of the OD layer, respectively.
151 It means that three orientations of the OD layer at 120° to one another will have
152 incompatible contacts.

153 The $P3_12$ structure is not an MDO polytype because it is generated by two above
154 outlined categories of operations in alternation, but it is a highly ordered structure:
155 the n th layer in the above defined starting orientation is propagated by the $2//a_{OD\ layer}$
156 operation into $(n+1)$ st layer, followed by the propagation of the $(n+1)$ st layer into
157 $(n+2)$ nd layer by the $2//(110)_{OD\ layer}$ (or $2//(1-10)_{OD\ layer}$ for the enantiomorph)
158 operation, *defined for the new orientation of the layer mesh*. Then the $(n+2)$ nd layer
159 is oriented towards the n th one by 120° . Continuing this two-term sequence of
160 symmetry operations, we obtain a $P3_12$ or $P3_22$ structure with a *six layer period*.

161 To summarize the preceding derivations, the crystal structure of vaterite is an OD
162 (order-disorder) structure composed of Ca-based OD layers with the symmetry $c2/m$.
163 These OD layers comprise the coordination polyhedra of calcium plus $1/2$ of the
164 height of the ‘standing’ CO_3 groups which interconnect two adjacent Ca-based layers,
165 both from the ‘top’ and from the ‘bottom’. Based on the configurations in the
166 carbonate layers ($p-62m$), the interlayer set of *sigma rho* operations relating the two
167 OD layers are three two-fold axes and the horizontal mirror of this layer group. *Sigma*
168 *tau* operations of the OD groupoid are c glide planes perpendicular to the particular

169 two-fold rotation axis. The resulting layer stackings with maximum degree of order
170 are $C2/c$, $P6_122$ and $P6_522$, $C2/c2/m2_1/m$ and a more complex variant, $P3_12$ ($P3_22$).
171 These maximally or highly ordered polytypes can be accompanied by more
172 complicated layer sequences and disordered variants which result from actions of
173 interlayer *sigma* symmetry operations with non-uniform or random orientations in the
174 layer stacking process.

175

176 Demichelis et al. (2013, Fig. 3) demonstrate that the ideal structures with the $C2/c$
177 and $P6_122$ symmetry have slightly higher internal free energy than $P3_121$, and they
178 undergo room-temperature distortions by means of minor rotation of carbonate
179 groups, to Cc , $C2$, $P6_1$ and $P2_1$, connected with a drop in internal free energy. The
180 energy differences they calculated, however, are small and they can be further
181 modified by presence of stacking faults so that they believe that natural vaterite is a
182 mixture of structures with different symmetries – which is a perfect expression of an
183 OD structure composed of layers.

184 As mentioned in the introduction, an alternative OD description of vaterite is
185 possible, as a structure composed of two kinds of OD layers, the Ca net alone as one
186 OD layer and the rest of the structure as another OD layer. The description as an OD
187 structure composed of two types of OD layers might be more universal but such a
188 description of vaterite is much more complicated and *less transparent* for a non-
189 specialist.

190 Some data quoted in the compilation of literature sources in Table 1 of Demichelis
191 (2013), none of which is concerned with their own work, are contradictory. The
192 $Pbnm$ structure (Meyer 1969) has $c = 8.5 \text{ \AA}$, but all cases with 6_3 screw axes (e.g.,
193 Meyer 1969) should have two-layer stacking periods. However, these cases cannot
194 exist with the here described OD layer. The $Pbnm$ proposal obtained through *ab initio*
195 calculations by Medeiros et al. (2007) differs in many substantial features from the
196 results of Wang and Becker (2009), Demichelis et al. (2012, 2013) and Mugnaioli et
197 al. (2012), and will not be treated here. The same is true for a different configuration
198 proposed by Le Bail et al. (2011) from powder diffraction data. The $4.1 \text{ \AA } a$ (i.e.,
199 one-layer) parameter of this $Ama2$ structure is strange.

200 During the time this paper was in preparation and review, several papers appeared
201 which appear to confirm our derivations. Kabalah-Amitai et al. (2013) found that

202 vaterite forming the spicules of the *Herdmania momus* ascidians predominantly
203 represents a hexagonal matrix with intervals of highly disordered layered structure
204 containing a component with unknown symmetry. This is a model in full agreement
205 with our derivations and with the suggestions by Demichelis et al. (2013). Wang et al.
206 (2014) performed molecular dynamics simulations which show that the $P6_522$
207 structure of Wang and Becker (2009) with ordered carbonate ions has internal energy
208 lower than the disordered structure. Their X-ray powder diffraction data fitted best
209 with this structure, although the reliability indices for the $C2/c$ and $P3_121$ were within
210 the acceptable range as well. Consistency with the $P6_522$ structure was also found for
211 the HRTEM observations. Burgess and Bryce (2015) used a combined ^{43}Ca solid-
212 state nuclear magnetic resonance spectroscopic and computational approach on
213 synthetic, ^{43}Ca – enriched vaterite samples, in combination with X-ray powder
214 diffraction. They suggest that their NMR and diffraction data favor the $P3_221$
215 structure and/or the monoclinic $C2$ structure whereas the $C2/c$ model yields an
216 excessively complicated powder pattern in comparison with the observed one. De La
217 Pierre et al. (2014) studied Raman spectra of vaterite, comparing the calculated and
218 experimental ones from a variety of materials. They found excellent agreement of
219 these spectra for the $P3_221$ structure and/or the monoclinic $C2(?)$ structure (these two
220 choices were practically indistinguishable) whereas the other symmetries yielded
221 additional minor Raman peaks not observed in the experimental material. If we
222 accept the $C2$ structure as a distorted derivative of the $C2/c$ model, the agreement of
223 all these observations with the OD derivations is very satisfactory.

224

225 The crystal structure of YbBO_3 (Bradley et al. 1966) is a distant homeotype of
226 vaterite. Yb cations form a hexagonal net, surrounded by the trigonal openwork of
227 BO_3 groups. The latter form hexagonal prisms which have 3 sides occupied by
228 triangles in a ‘rotation’ configuration, symmetry $3/m$, in combination with ditrigons
229 which house in- and out-pointing BO_3 triangles. Thus, YbBO_3 displays the same
230 basic scheme as vaterite. Cation coordination is different, however, pulling the
231 centers of ditrigons on one side of OD layer over the same type of centers on the
232 opposite side of the layer; they are related by inversion. This structure is an
233 introduction to the next group, from which it differs in important details.

234 **NEXT OF KIN: THE BATNÄSITE-SYNCHYSITE POLYSOMATIC SERIES**

235 The protracted efforts to solve the crystal structure of vaterite could have been
236 shortened by a close look at the known structures of the members of the bastnäsité -
237 synchysite polysomatic series of fluorocarbonates. This series,
238 $\text{Ca}_m(\text{REE})_n(\text{CO}_3)_{n+m}(\text{F},\text{OH})_n$ (Ferraris et al. 2008), with four well defined members
239 (bastnäsité, $m = 0, n = 1$; synchysite, $m = 1, n = 1$; parisite, $m = 1, n = 2$; röntgenite,
240 $m = 2, n = 3$), has been defined structurally by Donnay and Donnay (1953) and
241 subsequently refined by a number of researchers (Van Landuyt and Amelinckx 1975,
242 Yang et al. 1994, 1998, Ni et al. 2000). It became popular recently, in connection
243 with the world-wide exploration for *REE*. In these structures, all of which contain the
244 ‘standing’ CO_3 groups, a calcium-based layer alternates with a packet of one or
245 several *REE*-based layers. Yang et al. (1994, 1998) already noticed a relationship
246 between the Ca layers from the fluorocarbonates and vaterite, but as it was long
247 before the refinements by Demichelis et al. (2012, 2013) and Mugnaioli et al. (2012),
248 this observation did not receive due attention. We shall use the structure refinement
249 for *parisite* (Ni et al. 2000) to illustrate the relationship to the vaterite structure in
250 detail, in terms of layers configurationally close to those in vaterite.

251 In *parisite* (Fig. 5), a calcium-based layer alternates with a pack of two *REE*-based
252 layers. The Ca layer is identical with that described above as the vaterite OD layer. At
253 $z = 0$, the mirror plane of this $c2/m$ layer is parallel to (110) of the *parisite* cell. Unlike
254 the Ca layer, the *REE* layer also contains F atoms situated approximately (i.e.,
255 slightly above or below) in every triangle of the hexagonal *REE* net of cations. The
256 carbonate configurations surrounding the *REE* (i.e., cerium) layer are the same as
257 those surrounding the Ca layer but their mutual displacement across the hexagonal
258 *REE* net differs (Fig.6). The hexagons and ditrigons of the carbonate openwork on the
259 two sides of the *REE* layer are situated above one another in two settings: in two
260 thirds of cases, the $3/m\ 2\ m$ ditrigons with in- and outwards orientation of CO_3 groups
261 lie above or below the distorted $3/m$ hexagons with a ‘rotational’ arrangement of CO_3
262 groups, and in one third of cases, two oppositely pointing ‘rotational’ arrangements
263 share the same x,y coordinates, in a -3 arrangement (Fig. 6). The resulting layer
264 symmetry of the *REE layer* (configurationally analogous to the Ca-based OD layer) is
265 $p32$ whereas the general scheme according to which the different types of
266 hexagons/ditrigons are disposed is $p\ -3\ 2/m\ 1$ when we ignore the orientation of
267 triangular CO_3 groups.

268 The action of the potential OD *sigma rho* operations in the median plane of each
269 carbonate layer (the same as in vaterite), from which we can mention the three

270 twofold rotation axes at 120° to one another, does not lead to a polytypism in a Ca-
271 free sequence, as already stressed by Ni et al. (2000). For an *REE layer pair*, the
272 openwork hexagons of the $(n+1)$ st layer lie above those of the n th layer. The
273 hexagon sequences with counter-rotation of three CO_3 groups in the walls lie above
274 one another and the sequences of alternatively centripetal and rotational CO_3
275 arrangement in the walls again follow one another along the stacking direction. For
276 the Ca-free bastnäsite, this layer stacking symmetry results in the *P-32c* space group.
277 As already suggested by Ni et al. (2000), a linkage of two *REE* layers by a Ca layer
278 generates an offset between slabs; this offset is the origin of the observed polytypism
279 in the Ca-*REE* fluorocarbonates (Ferraris et al. 2008). Detailed treatment of the
280 polytypism of this series lies outside the scope of this paper. We should mention that
281 the stacking of different ditrigonal elements of the carbonate openwork in the
282 fluorocarbonate series and of the borate openwork in YbBO_3 (Bradley et al. 1966) is
283 completely different.

284 **IMPLICATIONS**

285
286 The derivations presented here demonstrate that polytypism and occurrence of
287 random stacking is an inherent property of vaterite.

288 Different polytypes will have very similar free energies, further reduced by relaxation
289 by slight distortions allowed by a particular space group or its subgroup. Stacking
290 faults produced in the OD process do not substantially alter the energy situation
291 either. Thus, the kinetics of random nucleation will have profound influence on the
292 resulting layer stacking, especially because vaterite is a result of (relatively) low-
293 temperature processes at (often) high reaction rates. The resulting crystals will have
294 high configurational entropy.

295 Although resulting in the same set of derived or potential vaterite polytype structures
296 as the study of Demichelis et al. (2012, 2013), the one-layer OD approach gives a
297 simpler and more transparent picture of vaterite polytypism than the scheme of
298 carbonate layer shifts and rotations used in the previous studies.

299 A fully developed vaterite-like ‘OD’ layer of the type defined and used in this study,
300 different from the rest of the structure, is present in the Ca-*REE* fluorocarbonates of
301 the bastnäsite - synchysite polysomatic series. On the one hand, it is *a cause of*
302 *polytypism* in this series and on the other hand it shows that *vaterite is, in all respects,*
303 *the extreme end-member of this series*, with the number of *REE* layers reduced to nil,

304 as already suggested by Yang et al. (1998). At present, no fluorocarbonates with
305 multiple vaterite-like layers, or vaterite with intercalated *REE* layers, are known but
306 their existence and character, especially as synthetic products, is predictable from the
307 current model.

308 **ACKNOWLEDGMENTS**

309 Dr. Raffaella Demichelis kindly supplied *cif* files of the vaterite variants derived in
310 their work. This paper contributed to the Nano-Chalk Venture, funded by Maersk Oil
311 and Gas A/S and the Danish Advanced Technology foundation (HTF). Discussions
312 with the members of the Nano-Geochemistry group, Nano-Science Center, University
313 of Copenhagen, chaired by Prof. Susan L.S. Stipp, were appreciated. I am grateful to
314 the associate editor, Dr. D.R. Hummer, and two anonymous referees for the helpful
315 comments.

316 **APPENDIX: BASIC NOTIONS OF THE THEORY OF OD PHENOMENA**

317 All crystal structures can be sectioned into equivalent slabs. For the majority of
318 structures, the orientation and position of the $(n+1)$ st slab after the n th slab is
319 unambiguously determined. The less frequent cases when these rules are relaxed but
320 still deterministic, are dealt with by the OD (order-disorder) theory. In the sense used
321 in this contribution, OD (order-disorder) phenomena describe ambiguity in the
322 position (and orientation) of the $(n+1)$ st slab of the structure after every n th slab. In
323 the OD structures, the two (or more) positional/orientational choices give rise to two
324 or several *geometrically (and thus also crystal-chemically) equivalent pairs of slabs*,
325 which differ from one another only by their orientation. These slabs are purely
326 geometrical and not always identical with crystal chemically defined layers. They are
327 called *OD layers*, with their own crystallographic (pseudo)symmetry, described by
328 one of the eighty layer groups [consisting of the so-called *intralayer* (or λ -) *partial*
329 *operations* (POs); the partial character of the operations means that they are not
330 necessarily valid for the whole structure; they may be valid only for the OD layer].
331 Another set of operations (the so-called *interlayer partial operations* or σ -POs)
332 transforms an OD layer into the adjacent one. Together these two kinds of operations

333 do not form a symmetry group but a weaker combination of symmetry operations, a
334 *groupoid* (Dornberger-Schiff, 1964). The above-mentioned positional ambiguity
335 means that – although all layer pairs are equivalent - layer triples, quadruples, etc.,
336 are not automatically identical even in one and the same structure or in various
337 crystals of the same substance. All OD-structures with the same set of λ -POs and σ -
338 POs to the exclusion of translations belong to one *OD-groupoid family*. Our case,
339 vaterite, is described as one of the families of OD structures composed of *one kind of*
340 *OD layers* but ample examples of OD structures composed of two (or more) kinds of
341 OD layers in regular alternation exist as well (e.g., Ferraris et al. 2008).

342

343 The partial character of interlayer operations (glide-reflection planes and screw axes)
344 in the OD structures involves unusual translation components with special notation
345 rules. In all cases the translation component is referred to the basis vectors of the OD
346 layer. Generalized notation rules for partial symmetry operations which interconnect
347 an *n*th layer with the (*n*+1)st layer (σ -POs) are as follows: for a glide plane, *the*
348 *translation component* is the value of the subscript attached to the symbol divided by
349 two: n ($\equiv n_1$) has translation equal to $\frac{1}{2}$ of the full translation vector, $n_{\frac{1}{2}}$ has
350 translation component equal to $\frac{1}{4}$ of the translation vector, n_2 has a translation
351 component equal to a full translation period (from one OD layer to the next one), etc.
352 In a similar way, 2_1 has the translation component equal to $\frac{1}{2}$ of the full translation
353 period parallel to the axis, 2_2 is a partial operation with the translation equal to a full
354 translation period of the lattice along the given axis, etc.

355

356

REFERENCES CITED

357 Bradley, W.F., Graf, D.L., and Roth, R.S. (1966) The vaterite-type ABO_3 rare-earth
358 borates. Acta Crystallographica, 20, 283-287.

- 359 Burgess, K.M.N., and Bryce, D.L. (2015): On the crystal structure of the vaterite
360 polymorph of CaCO₃: A calcium-43 solid-state NMR and computational assessment.
361 Solid State Nuclear Magnetic Resonance, 65, 75-83.
- 362 De La Pierre, M., Demichelis, R., Wehrmeister, U., Jacob, D.E., Raiteri, P., Gale,
363 J.D., and Orlando, R. (2014): Probing the multiple structures of vaterite through
364 combined computational and experimental Raman spectroscopy. Journal of Physical
365 Chemistry C, 118, 27493-27501.
- 366 Demichelis, R., Raiteri, P., Gale, J.D., and Dovesi, R. (2012) A new structural model
367 for disorder in vaterite from first-principles calculations. Crystal Engineering
368 Communications, 14, 44-47.
- 369 Demichelis, R., Raiteri, P., Gale, J.D., and Dovesi, R. (2013) The multiple structures
370 of vaterite. Crystal Growth and Design, 13, 2247-2251.
- 371 Donnay, G., and Donnay, J.D.H. (1953) The crystallography of bastnäsite, parisite,
372 röntgenite and synchisite. American Mineralogist, 38, 932-963.
- 373 Dornberger-Schiff, K. (1956) On the order-disorder structures (OD-structures). Acta
374 Crystallographica, 9, 593-601.
- 375 Dornberger-Schiff, K. (1966) Lehrgang über OD-Strukturen. Akademie-Verlag,
376 Berlin.
- 377 Āuroviĉ, S. (1997) Fundamentals of the OD theory. EMU Notes in Mineralogy, 1, 3-
378 28.
- 379 Ferraris, G., Makovicky, E., and Merlino, S. (2008) Crystallography of modular
380 materials. Oxford University Press.
- 381 Kabalah-Amitai, L., Mayzel, B., Kauffmann, Y., Fitch, A.N., Bloch, L. Gilbert,
382 P.U.P.A., and Pokroy, B. (2013): Vaterite crystals contain two interspersed crystal
383 structures. Science, 340, 454-457.
- 384 Le Bail, A., Ouhenia, S., and Chateigner, D. (2011) Microtwinning hypothesis for a
385 more ordered vaterite model. Powder Diffraction, 26, 16 - 21
- 386 Medeiros, K., Albuquerque, E.L., Maia, F.F.Jr., Caetano, E.W.S., and Freire, V.N.
387 (2007) First-principles calculations of structural, electronic and optical absorption
388 properties of CaCO₃ vaterite. Chemical Physics Letters, 435, 59 – 64

- 389 Merlino, S. (1997) OD approach in minerals: examples and applications. EMU Notes
390 in Mineralogy, 1, 29-54.
- 391 Meyer, H.J. (1969) Struktur und Fehlordnung des Vaterits. Zeitschrift für
392 Kristallographie, 128, 183-212.
- 393 Mugnaioli, E., Andrusenko, I., Schüler, T., Loges, N., Dinnebier, R.E., Panthöfer, M.,
394 Tremel, W., and Kolb, U. (2012) Ab initio structure determination of vaterite by
395 automated electron diffraction. Angewandte Chemie, International Edition, 51, 7041-
396 7045.
- 397 Ni, Y., Post, J.E., and Hughes, J.M. (2000) The crystal structure of parisite-(Ce),
398 $\text{Ce}_2\text{CaF}_2(\text{CO}_3)_3$. American Mineralogist, 85, 251-258.
- 399 Van Landuyt, J., and Amelinckx, S. (1975) Multiple beam direct lattice imaging of
400 new mixed-layer compounds of the bastnäsite – synchysite series. American
401 Mineralogist, 60, 351-358.
- 402 Wang, J., and Becker, U. (2009) Structure and carbonate orientation of vaterite
403 (CaCO_3). American Mineralogist, 94, 380-386.
- 404 Wang, J., Zhang, F., Zhang, J., and Ewing, R.C. (2014): Carbonate orientational
405 order and superlattice structure in vaterite. Journal of crystal Growth, 407, 78-86.
- 406 Yang, Z., Pan, Z., and Wu, X. (1994) Transmission electron microscope study of the
407 new regular stacking structure in the calcium rare-earth fluorcarbonate mineral series
408 from southwest China. Scientia Geologica Sinica, 29, 393-398 (in Chinese).
- 409 Yang, Z., Tao, K., and Zhang, P. (1998) The symmetry transformations of modules in
410 bastnäsite – vaterite polysomatic series. Neues Jahrbuch für Mineralogie,
411 Monatshefte, 1-12.

412 **FIGURE CAPTIONS**

- 413 **FIGURE 1.** The $C2/c$ structure of vaterite according to Mugnaioli et al. (2012). Large
414 spheres: Ca, triangles: CO_3 groups. (001) plane is horizontal, c axis subvertical.
- 415 **FIGURE 2.** Configuration of the carbonate layer on one side of the calcium net of
416 vaterite (from the $P6_522$ structure defined by Demichelis *et al.* (2012)). Grey
417 spheres: Ca, triangles: CO_3 groups. Oblique view was selected in order to make the
418 ‘standing’ CO_3 groups visible. The carbonate layer consists of a trigonal openwork of

419 CO₃ groups with distorted hexagons decorated by three triangles in a rotating
420 arrangement and of ditrigons with three inward and three outward oriented CO₃
421 triangles. The latter surround on three sides the configuration in which the axial cross
422 has been placed.

423 **FIGURE 3.** The OD layer derived from the *P6₅22* crystal structure variant of vaterite
424 (Demichelis et al. 2012), valid for all polytypes treated in this paper. It consists from
425 the central net of Ca atoms and the adjacent halves of standing triangular CO₃ groups.
426 However, for the sake of legibility, entire CO₃ groups are shown. In the present
427 orientation, the mirror plane of the *c2/m* layer group of the OD layer is parallel to (1-
428 100) of the hexagonal cell. Oblique view was selected in order to make the ‘standing’
429 CO₃ groups visible.

430 **FIGURE 4A,B.** Different orientations of the interlayer symmetry operations (*sigma*
431 operations; here the horizontal polar two-fold rotation axes indicated by short arrows)
432 in relation to the centered unit mesh and the symmetry elements of the adjacent OD
433 layer. (a) Action of a *sigma* operation (a two-fold rotation axis indicated by an arrow)
434 generating the 6₅ and *C2/c* polytypes, and (b) action of the *sigma* operation (right-left
435 oriented two-fold axis) generating the orthorhombic 2-layer polytype. Compare with
436 description in the text.

437 **FIGURE 5.** The crystal structure of parisite (Ni et al. 2000). Grey spheres: Ca, black
438 spheres: *REE*, white large spheres: F, and triangles: ‘standing’ CO₃ groups with
439 oxygen as small spheres in the corners. (001) planes are viewed edge-on, the *a* axis
440 points approximately to the left, *c* axis is subvertical

441 **FIGURE 6.** The *REE*-based layer from the crystal structure of parisite: the cation net
442 with halves of attached carbonate groups. For clarity of design, however, entire CO₃
443 groups are shown. For conventions see Fig. 5.

444

445

446

447

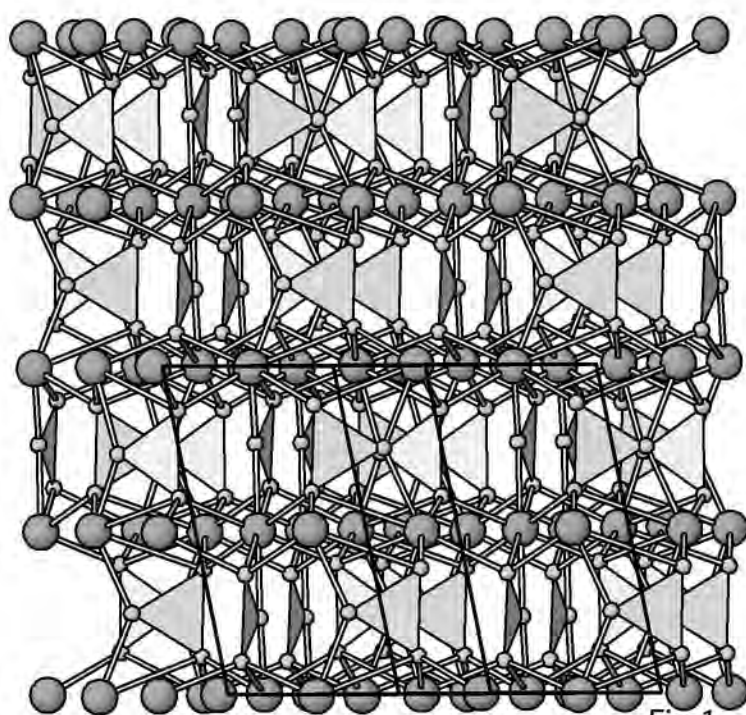
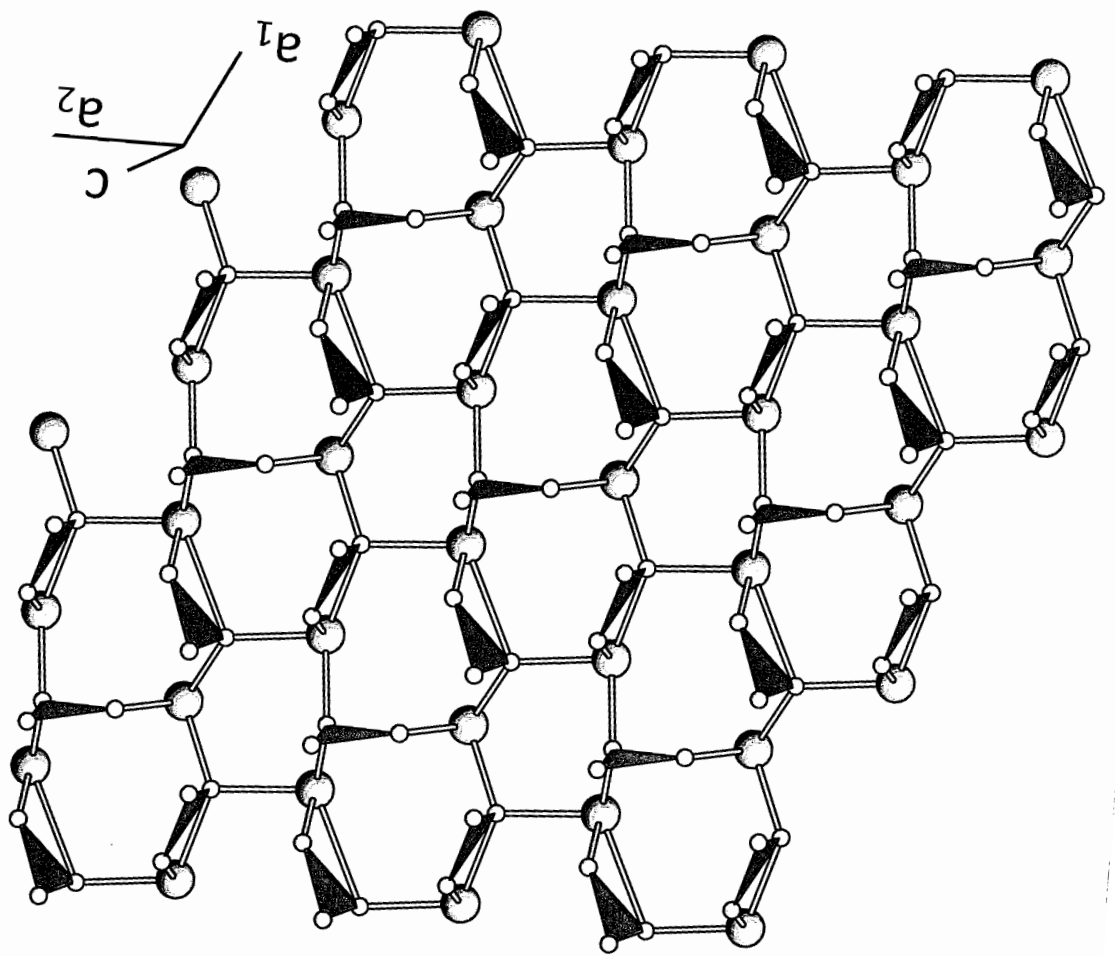
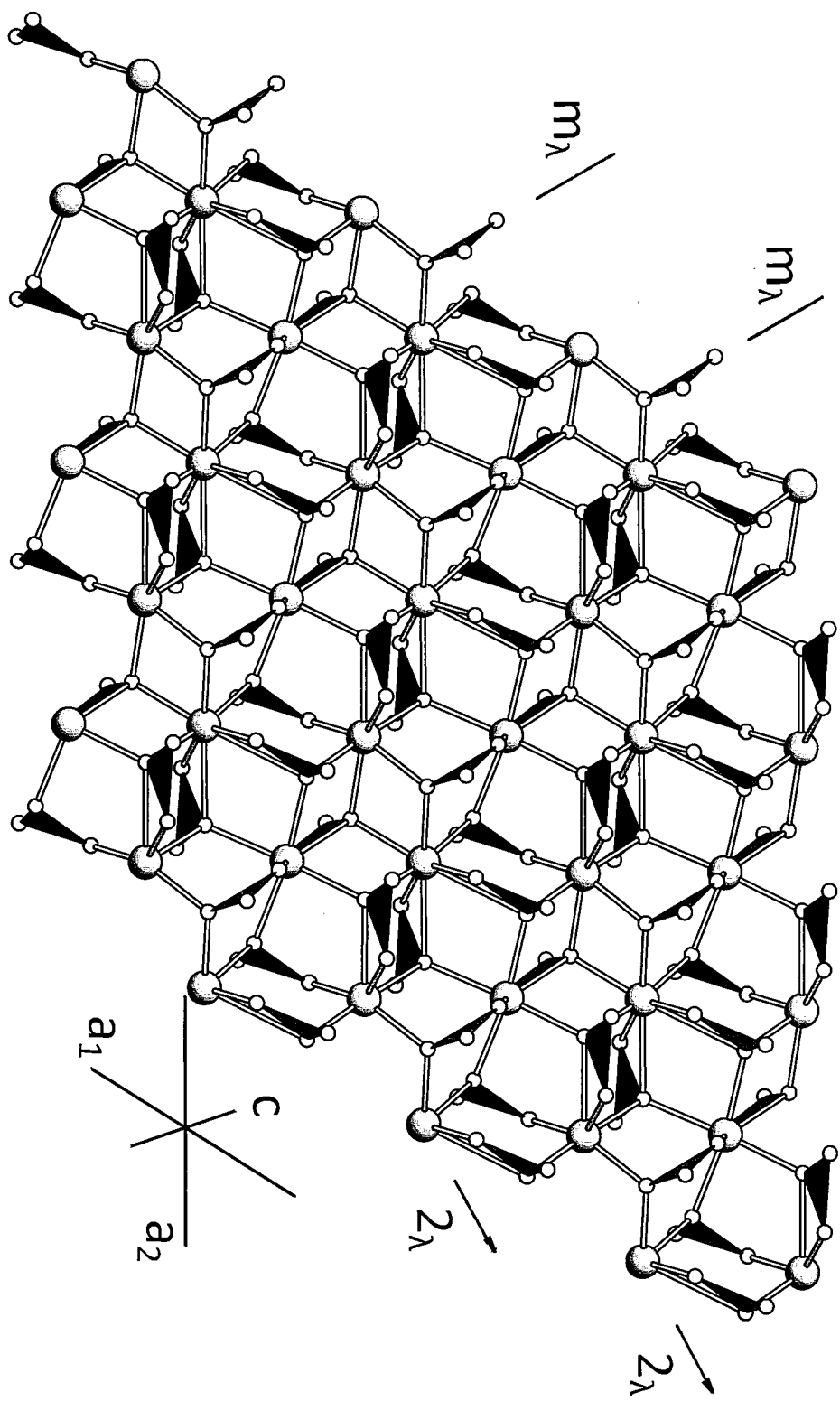
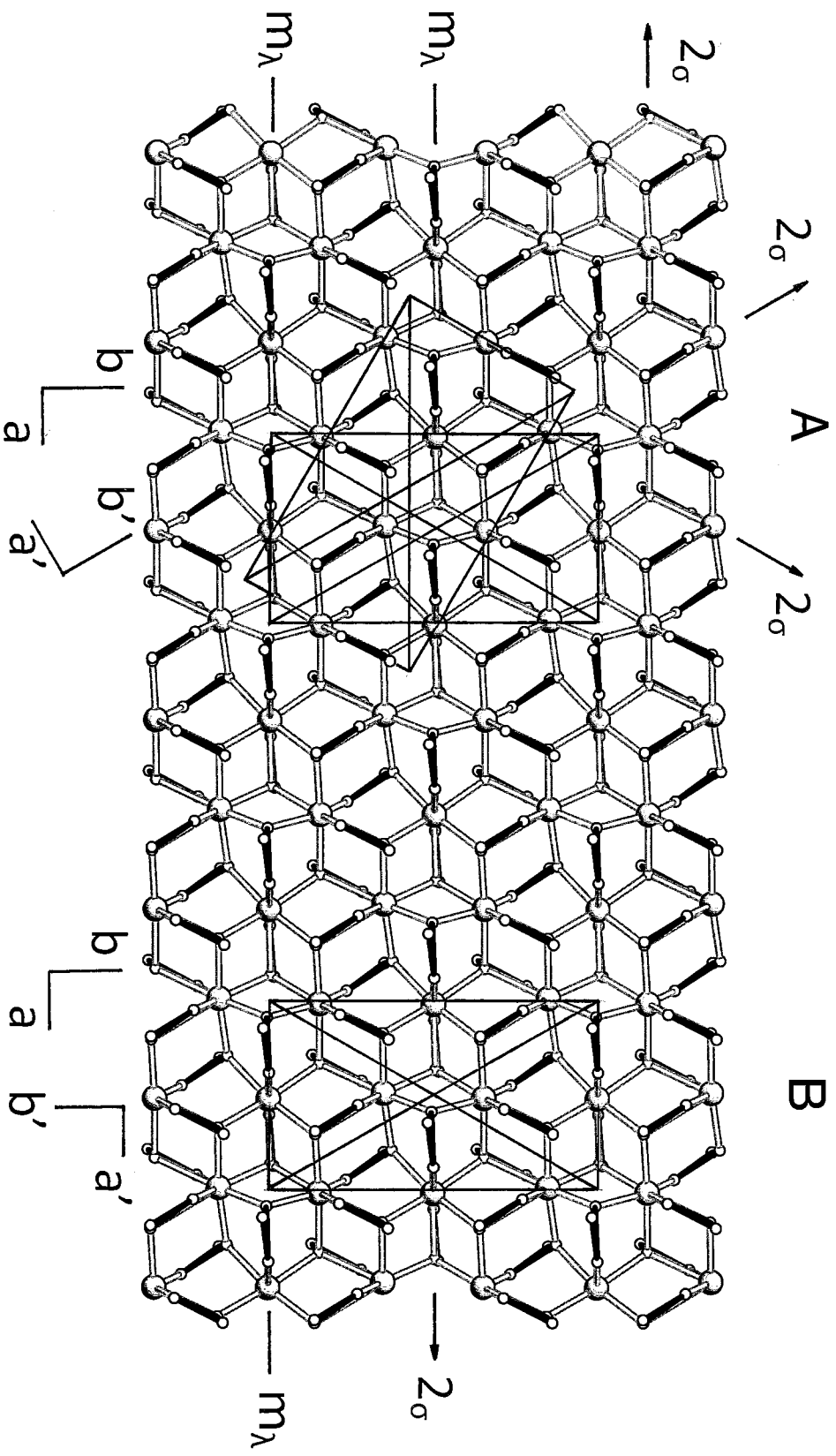


Fig.1







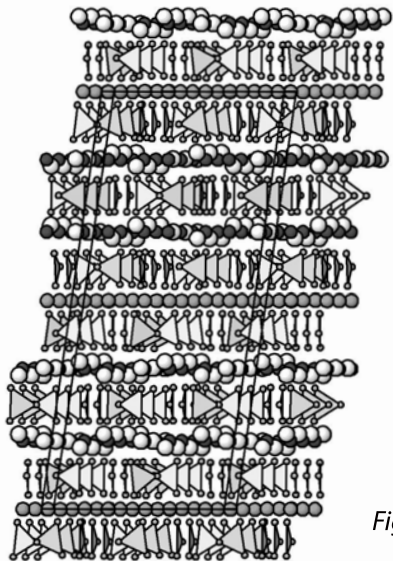


Fig.5

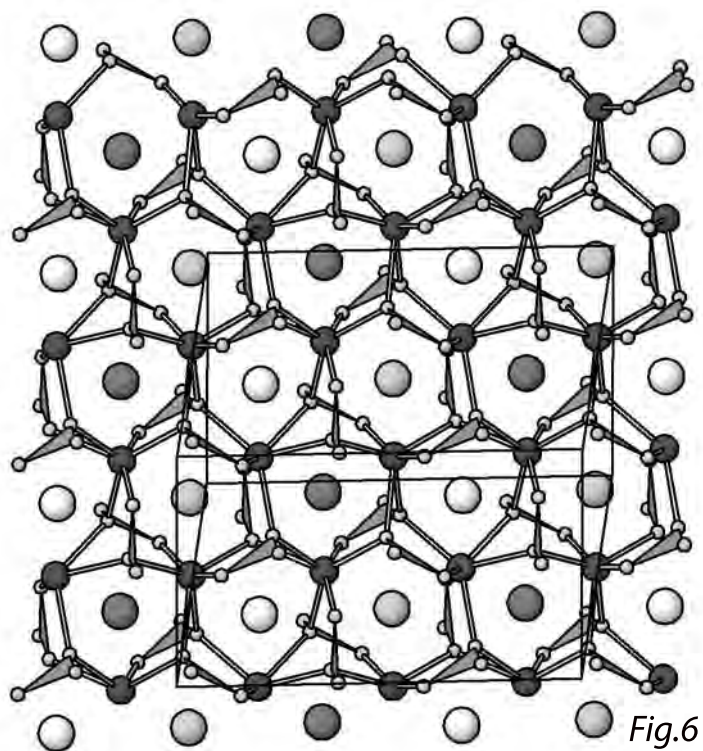


Fig.6